XI. APPLIED PLASMA RESEARCH*

A. Active Plasma Systems

Academic and Research Staff

Prof. L. D. Smullin
Prof. R. J. Briggs
Prof. R. R. Parker
Prof. K. I. Thomassen

Graduate Students

Y. Ayasli
D. S. Guttman
B. R. Kusse
R. K. Linford
J. A. Mangano
J. A. Rome
M. Simonutti

1. INSTABILITY THEORY AND NONUNIFORM MEDIA

A problem of considerable general importance in plasma stability theory is the development of techniques for handling inhomogeneous media. The Wentzel-Kramers-Brillouin (WKB) approximation has been frequently used in the past to get some idea of the effects of inhomogeneities and finite size on the instabilities predicted by uniform media analyses.[1-3] The major aim of this work has been the construction of discrete normal modes, with associated phase integral expressions for determining the eigenfrequencies. It is clear that the confinement of attention to the eigenmode problem leaves many important questions unanswered. For instance, if the system is large but only slightly inhomogeneous, is there a branch line in the Laplace-transformed Green's function, $\psi(\omega, z)$, as is the case for an infinite uniform medium?[4] In this report, we shall exhibit and analyze a simple example (drawn from mode-coupling theory) that illustrates some subtleties in the application of WKB methods to unstable media, and also emphasizes the importance of considering the full source problem in a complete stability treatment.

Mode-Coupling Example

For a time-invariant medium, we can introduce the Laplace transform of the response function $\psi(t, z)$,

$$\psi(\omega, z) = \int_0^\infty \psi(t, z)\, e^{-j\omega t}\, dt. \tag{1}$$

We take a source function of the form $\delta(t)\,\delta(z)$ (the generalization to an arbitrary position z' of the source is straightforward but will not be carried out here) and consider the case for which the differential equation for $\psi(\omega, z)$ is of the form

*This work was supported by the National Science Foundation (Grant GK-10472); additional support was received from the Joint Services Electronics Programs (U.S. Army, U.S. Navy, and U.S. Air Force) under Contract DA 28-043-AMC-02536(E).

$$\frac{\partial^2 \psi(\omega, z)}{\partial z^2} + Q(\omega, z)\, \psi(\omega, z) = -\delta(z), \tag{2}$$

with

$$Q(\omega, z) = \frac{1}{v^2}(\omega + \beta z)^2 + K_o^2(1 - z^2/L^2). \tag{3}$$

The local dispersion relation is clearly

$$k^2(\omega, z) = Q(\omega, z), \tag{4}$$

where k is the spatially varying wave number in the z direction. In a "local" sense, this example corresponds to a medium that is absolutely unstable in the region

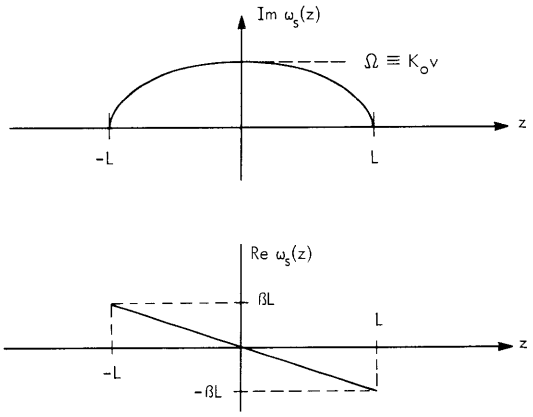

Fig. XI-1. Solution to local dispersion relation (local pinch frequency), $Q(\omega, z) = 0$. The medium is stable for $|z| \geq L$, and the majority of the analysis is carried out for the case in which the real part of the instability frequency is detuned over a length L by an amount equal to the maximum growth rate ($\beta L \leq \Omega$).

$-L < z < L$ and stable for $|z| > L$. (See Fig. XI-1.)

The (local) pinch occurs when $k = 0$, and at the frequency

$$\omega_s(z) = -\beta z \pm jK_o v \sqrt{1 - z^2/L^2}. \tag{5}$$

Note that this "local pinch frequency" is the same as the solution to what is sometimes referred to as the "local dispersion relation," $Q(\omega, z) = 0$. [In physical cases when this example arises, the actual frequency and wave number ($\tilde{\omega}$ and $\tilde{k}$) could be shifted from the origin, that is, $\tilde{\omega} = \omega - \omega_o$ and $\tilde{k} = k - k_o$, where ω_o and k_o are the real frequency and

wave number where the modes couple.[5] The over-all response would thus be multiplied by a factor exp $j(\omega_o t - k_o z)$.] The "local absolute growth rate" is thus a maximum at $z = 0$ and goes to zero at $z = \pm L$, while the real part of the pinch frequency is detuned linearly with z.

The case of no "detuning" ($\beta \equiv 0$) was considered in an earlier report where it was shown that WKB normal modes can be formed with the eigenfrequencies[3]

$$\frac{\omega^2}{v^2} = (2n+1)\frac{K_o}{L} - K_o^2, \tag{6}$$

where $n = 0, 1, 2, 3, \ldots$. All normal modes are thus stable if

$$L < L_{crit} = \frac{1}{K_o}. \tag{7}$$

In this report, we shall develop the complete response function (solution to Eq. 2) for the special choice

$$\beta = \frac{K_o v}{L} \equiv \frac{\Omega}{L}. \tag{8}$$

This choice of β makes Q linear in z, since then

$$\begin{aligned} Q(\omega, z) &= \frac{\omega^2}{v^2} + K_o^2 + 2\frac{\omega}{v}\frac{K_o}{L} z \\ &= A(\omega) + B(\omega)\, z. \end{aligned} \tag{9}$$

For a linear variation of Q, there is no possibility of "trapped modes" (discrete normal modes) in the WKB sense, since there is only one turning point. Thus this special choice of β will most clearly illustrate effects other than the discrete normal-mode excitation.

Exact Solution for the Response

An exact solution for $\psi(\omega, z)$ can be obtained by Fourier-transforming $\psi(\omega, z)$ (possible certainly for $\omega_i < -\Omega$ because the medium is stable for $|z| > L$):

$$\psi(\omega, k) = \int_{-\infty}^{+\infty} \psi(\omega, z)\, e^{jkz}\, dz \tag{10}$$

$$\psi(\omega, z) = \int_{-\infty}^{+\infty} \psi(\omega, k)\, e^{-jkz}\, \frac{dk}{2\pi}. \tag{11}$$

This yields the following first-order differential equation for $\psi(\omega, k)$ from (2).

$$\frac{\partial\psi(\omega,k)}{\partial k} + \frac{j}{B}(A-k^2)\,\psi(\omega,k) = -\frac{j}{B}, \tag{12}$$

with the solution

$$\psi(\omega,k) = -\frac{j}{B}\int_{-\infty}^{k} dq\, \exp\left\{\frac{j}{B}\left[A(q-k) - \frac{1}{3}(q^3-k^3)\right]\right\}. \tag{13}$$

A detailed argument shows that the lower limit of $-\infty$ on the integration over q is necessary to insure the analyticity of $\psi(\omega, k)$ in the lower-half ω-plane, $\omega_i < -\Omega$.

A change of variables from q to u, where

$$q = k - u, \tag{14}$$

results in an exponent that is only quadratic in k. By inserting this expression for $\psi(\omega, k)$ into (11), the integration over k can be performed, and we obtain

$$\psi(\omega, z) = \frac{1}{2}\int_0^{\infty} du\, (j\pi Bu)^{-1/2}\, \exp\{F(u)\}, \tag{15}$$

where

$$F(u) = \frac{1}{jB}\left\{-\frac{u^3}{12} + u\left(A + \frac{Bz}{2}\right) + \frac{B^2z^2}{4u}\right\}. \tag{16}$$

The expression for $\psi(\omega, z)$ is valid only for $\omega_i \leq 0$, and the correct branch of $(jB)^{1/2}$ is the one with a positive real part.

The final desired result is the response function $\psi(t, z)$ which is obtained from the inverse Laplace transform:

$$\psi(t, z) = \int_{-\infty-j\sigma}^{+\infty-j\sigma} \psi(\omega, z)\, e^{j\omega t}\frac{d\omega}{2\pi}. \tag{17}$$

Equations 15-17 represent an exact formal solution to the problem that we posed. Notice that we have not made any assumptions up to this point about the scale of inhomogeneity (L). We know that for the infinite system ($L = \infty$), the function $\psi(\omega, z)$ has a branch point in the ω-plane at $\omega = -j\Omega$ (cf. Eq. 5 and Fig. XI-1), and this leads to an asymptotic growth[4] of $\exp(\Omega t)$ for $\psi(t, z)$. In the present case, for any $L \neq \infty$ we see from the integral expression (Eq. 15) for $\psi(\omega, z)$, together with the definitions of $A(\omega)$ and $B(\omega)$ in Eq. 9, that $\psi(\omega, z)$ is analytic in the entire lower-half ω-plane, with the exception of an essential singularity (and branch point) at $\omega = 0$. The analytic behavior of $\psi(\omega, z)$ in the complex ω-plane is thus entirely different in the inhomogeneous case,

no matter how weak the inhomogeneity is. Physically, we certainly expect the nature of the actual time-dependent response, $\psi(t, z)$, to be very similar to the uniform media response in the limit of large L. To show this, we shall now evaluate $\psi(t, z)$ at $z = 0$ by a saddle-point technique.

The expression for $\psi(t, 0)$ as given by Eqs. 15-17 is of the form

$$\psi(t, 0) = \int_{-\infty-j\sigma}^{+\infty-j\sigma} \frac{d\omega}{2\pi} \int_0^\infty du \, \frac{1}{2} (j\pi Bu)^{-1/2} \exp[G(u, \omega, t)]. \tag{18}$$

The limiting form of $\psi(t, 0)$ is governed by the saddle points of G in $(\omega\text{-}u)$-space, where $\frac{\partial G}{\partial u} = 0$, and $\frac{\partial G}{\partial \omega} = 0$. We find that these saddle points are located along the imaginary ω axis ($\omega = j\omega_i$), and in terms of the normalized variables $y = -\omega_i/\Omega$, $u_n = u/K_o$, the saddle points are determined by

$$u_n = 2\sqrt{1 - y^2}, \tag{19}$$

where

$$(1-y^2)^{1/2} \left[\frac{2}{3} \frac{1}{y^2} + \frac{4}{3}\right] = \frac{vt}{L}, \tag{20}$$

and G is given by

$$G(u_n, y) = K_o L \left[y \frac{vt}{L} + \frac{1}{2y} \left(u_n - \frac{u_n^3}{12} - u_n y^2 \right) \right]. \tag{21}$$

It can be shown that the path of integration in $(\omega\text{-}u)$-space can be deformed to pass through the appropriate saddle point in the direction of steepest descent. For $vt/L \ll 1$, the saddle points are near $y \approx 1$ ($\omega_i \approx -\Omega$) and $G \approx \Omega t$ at the saddle. In this regime we have growth at essentially the infinite media rate (Fig. XI-2). For $vt/L \gg 1$, however, the saddle point moves toward the origin in the ω-plane ($y \ll 1$) and we obtain the asymptotic growth

$$\psi(t, 0) \sim \exp\left[2 \left(\frac{2}{3} K_o L \Omega t \right)^{1/2} \right]. \tag{22}$$

That is, $\psi(t, 0)$ grows as $\exp(C\sqrt{t})$ for large time (see Fig. XI-2). These results are entirely reasonable. The velocity v is physically the "wavefront" velocity in this medium, since $\omega/k \sim \pm v$ for large ω. Therefore, our results indicate that the disturbance initially grows at the infinite uniform media rate until the disturbance can propagate over the inhomogeneity scale length, L. After this critical time L/v, the disturbance grows more slowly, since the "leakage" of signal to the adjacent stable medium begins to be felt. Naturally, if $\Omega L/v = K_o L$ is very much larger

than unity, nonlinear effects will set in well before the finite-size effects are of any consequence. An even more important observation, however, is the fact that asymptotic growth as given by Eq. 22 obtains even for "small systems" with $K_o L \ll 1$. For the case of no "detuning" ($\beta = 0$), which was discussed earlier, the normal modes were all stable if $K_o L < 1$. The present case has no discrete normal modes (isolated poles of $\psi(\omega, z)$); however, we find asymptotic growth for any system size, which is rather surprising.

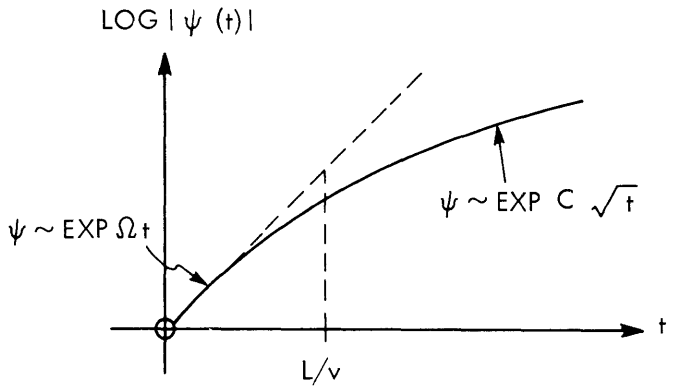

Fig. XI-2. Growth of $\psi(t, z = 0)$.

A Modification to the Example

The asymptotic growth $\exp(C\sqrt{t})$ can be traced to the existence of an essential singularity of $\psi(\omega, z)$ on the real ω axis.[6] If we modify the example above by replacing ω with $\omega - j\upsilon$ everywhere (introducing "loss" in the coupled-wave system[5]), then the essential singularity is shifted up to $\omega = j\upsilon$, and $\psi(\omega, z)$ is analytic in the entire lower-half ω-plane and along the real $-\omega$ axis. We then know that the impulse response will eventually decay as $t \to \infty$; it can be easily shown that the modification in Eq. 22 amounts to a multiplication by $\exp(-\upsilon t)$, and therefore the decaying exponential dominates for large enough t, even with very small υ.

Since we now have a "stable" system, it seems clear that all essential information should be contained in the behavior of $\psi(\omega, z)$ for real ω. (If we drove the system with a sinusoidal signal at a (real) frequency ω_s, then the asymptotic response would be $\psi(\omega_s, z) \exp(j\omega_s t)$ for large time.) With υ very small, however, ($\upsilon \ll \Omega$) local wave numbers given by (4) are essentially pure real for real ω in the unstable ($|z| < L$) region. Thus, any signal "amplification" cannot be due to spatial growth of the signal, as contained in factors such as $\int_{z_o}^{z} \text{Im } k(\omega, z)\, dz$ which are certainly of order υ. Indeed, what

we shall show is that $\psi(\omega, z)$ for real ω is essentially constant in z but exponentially large everywhere. Any excitation of the system (by noise) would therefore lead to very large-amplitude fluctuations with a "flat" spatial structure.

If we replace ω with $\omega - j\upsilon$ in the expressions for $A(\omega)$ and $B(\omega)$ in (9), and assume that $\omega \sim \upsilon \ll \Omega$ and $|z| \ll \frac{\Omega}{\upsilon} L$, then a saddle-point evaluation of $\psi(\omega, z)$ as given in (15) yields

$$\psi(\omega, z) \sim \exp\left[\frac{2}{3} \frac{\Omega K_o L}{(\upsilon + j\omega)}\right] \tag{23}$$

(outside of various multiplicative factors). The steady-state response to a sinusoidal drive at z = 0 is, therefore, a maximum at $\omega = 0$ (with a bandwidth the order of υ) and is essentially independent of z over the domain $|z/L| < \Omega/\upsilon$, which verifies the statements above.

Interpretation of Results by a WKB Development

We derived the preceding results by taking asymptotic limits of an exact integral expression for the impulse response. Our main reason for proceeding in this way was to determine clearly whether or not there were any branch cuts in $\psi(\omega, z)$. The results that we have derived, however, can be obtained directly from a WKB approximation, as would be expected because the asymptotic limits of the integral representation should reduce to essentially the WKB solutions.

Let us define the two WKB solutions to the homogeneous equation (ignoring slowly varying multipliers) as

$$\psi_1(\omega, z) = \exp j \int_{z_o}^{z} k(\omega, z)\, dz \tag{24}$$

$$\psi_2(\omega, z) = \exp -j \int_{z_o}^{z} k(\omega, z)\, dz, \tag{25}$$

where

$$\int_{z_o}^{z} k(\omega, z)\, dz = \int_{z_o}^{z} (A+Bz)^{1/2}\, dz \tag{26}$$

$$= \frac{2}{3B} (A+Bz)^{3/2} \tag{27}$$

and

$$z_o = -A/B \tag{28}$$

is the turning point (see Fig. XI-3). For purely imaginary ω, the turning point is along the imaginary z axis. With $\omega_i < -\Omega$, the turning point is in the upper-half z-plane; as $-\omega_i$ falls below Ω, it hits the axis ($z = 0$) and goes into the lower-half z-plane.

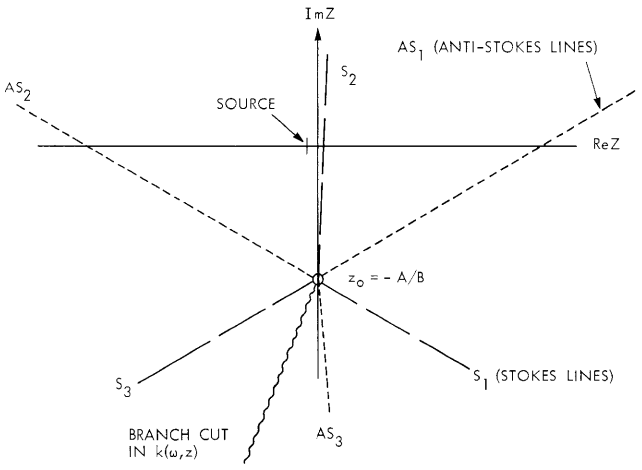

Fig. XI-3.
Stokes lines for ψ_1 and ψ_2 in the complex z-plane. Along S_1, ψ_1 is dominant; along S_2, ψ_1 is subdominant; and along S_3, ψ_1 is again dominant, while the opposite applies to ψ_2. The sketch is for purely imaginary ω, with $-\Omega < \omega_i < 0$.

Let us now consider the example previously discussed, with $\omega \to \omega - j\upsilon$ and $\upsilon \ll \Omega$ in the expressions for A and B. For $z \to +\infty$, we find that ψ_2 is the subdominant solution and hence

$$\psi_+(\omega, z) = c_1\psi_2(\omega, z) \tag{29}$$

for $z > 0$. Just to the left of the Stokes line S_2 in Fig. XI-3 (and still to the right of the source, where we now assume that the source is located slightly to the left of $z = 0$), the solution picks up a contribution from the subdominant term (ψ_1),

$$\psi_+(\omega, z) = c_1(\psi_2 + j\psi_1). \tag{30}$$

In the regime $z \to -\infty$, ψ_2 is again the subdominant solution and hence to the left of the source we have

$$\psi_-(\omega, z) = c_2\psi_2. \tag{31}$$

The boundary conditions require

$$\psi_+ = \psi_- \tag{32}$$

$$\psi_+' - \psi_-' = -1 \tag{33}$$

at $z = z_s$, the source position. Since ψ_2 is dominant around $z \approx 0$, and the turning point z_o is very far from the axis, we must have

$$c_1 \approx c_2 = \frac{\psi_2(0)}{2k(0)}. \tag{34}$$

Along the real z axis therefore $\left(\text{with } |z| \ll \left|\frac{A}{B}\right|\right)$, the wave amplitude is the order of

$$\psi(\omega, z) \sim [\psi_2(z=0)]^2$$

$$\sim \exp\left(\frac{-4jA^{3/2}}{3B}\right),$$

in precise agreement with Eq. 23. The essential point of this example is that an arrangement of Stokes lines like that shown in Fig. XI-3 can give rise to a response that is extremely large (the square of the dominant solution), even with a turning point located very far from the real z axis. Without considering a source problem, of course, we would never uncover this behavior, since with one turning point it is clear at the outset that there are no eigenmodes.

R. J. Briggs

References

1. (a) H. L. Berk, L. D. Pearlstein, J. D. Callen, C. W. Horton, and M. N. Rosenbluth, Phys. Rev. Letters 22, 876-879 (1969).

   (b) H. L. Berk, T. K. Fowler, L. D. Pearlstein, R. F. Post, J. D. Callen, C. W. Horton, and M. N. Rosenbluth, Proc. Third International Conference on Plasma Physics and Controlled Nuclear Fusion Research, Novosibirsk, U.S.S.R., August 1968, Paper CN-24/G-12.

2. H. L. Berk and D. L. Book, Phys. Fluids 12, 649-661 (1969).

3. R. J. Briggs, Quarterly Progress Report No. 88, Research Laboratory of Electronics, M.I.T., January 15, 1968, pp. 186-192.

4. R. J. Briggs, Electron Stream Interaction with Plasmas (The M.I.T. Press, Cambridge, Mass., 1963).

5. D. L. Bobroff and H. A. Haus, J. Appl. Phys. 38, 390-403 (1967).

6. R. J. Briggs, Quarterly Progress Report No. 85, Research Laboratory of Electronics, M.I.T., April 15, 1967, pp. 183-185.

XI. APPLIED PLASMA RESEARCH*

B. Plasma Effects in Solids

Academic Research Staff

Prof. G. Bekefi
Prof. G. A. Baraff

Graduate Students

E. V. George
C. S. Hartmann
D. A. Platts
R. N. Wallace

1. MICROWAVE EMISSION FROM INDIUM ANTIMONIDE LOOPS

Further studies have been made of the X-band microwave emission produced by indium antimonide loops subjected to DC magnetic and RF electric fields. The basic experiment has been described in previous reports.[1,2] The results obtained here lend support to the view that the "low-field" microwave emission originally reported by Buchsbaum, Chynoweth, and Feldmann[3] was the result of phenomena taking place at or near the contacts of the samples tested.

Indium Antimonide Samples

All samples used in this work were cut from single crystals of n-type InSb having electron concentration in the range $1\text{-}2 \times 10^{14}/\text{cm}^3$ and electron mobility near 6×10^5 $\text{cm}^2/\text{V-sec}$ at 77°K. Both round and square loops were employed. Typical dimensions for each type of sample are shown in Fig. XI-4.

The square loops were cut by techniques previously described.[1] The plane of each

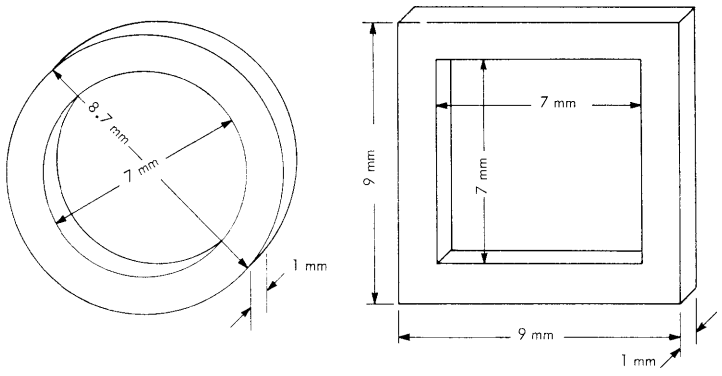

Fig. XI-4. Typical dimensions of square- and round-loop samples.

*This work was supported by the National Science Foundation (Grant GK-10472).

square lay in the (111) crystallographic plane, and one edge of each square was cut parallel to the $[\bar{1}10]$ axis. The round loops were cut with an abrasive drilling machine designed and constructed by D. A. Platts. Of the 4 round loops tested, 3 were cut so that the plane of the loop lay in the (111) plane; however, the placement of the $[\bar{1}10]$ axis in this plane was not recorded. The orientation of the fourth round loop was unknown. All samples were etched in a solution of bromine and methanol after the cutting process.

Two of the square loops were cut apart and soldered together as shown in the second report on this work.[4] For one sample, pure indium solder was used to join the separate parts of the loop; for the other sample, joints were formed with Wood's metal after the sample surfaces had been locally electroplated with tin. In past work, these soldering techniques have produced joints that apparently were ohmic. The behavior of these samples observed in the experiments suggests, however, that the contacts formed were not "good" in the sense recently described by George.[5]

Experimental System

The experimental system used for the work reported here is essentially the same as that described in the second report of this series.[2] The principal change is that the waveguide shown in that report[6] has been replaced by an eccentric transmission line which has a nominal characteristic impedance of 50 Ω. Indium antimonide loops are mounted on teflon supporting blocks that place the plane of the loop in the cross-sectional plane of the transmission line. These new transmission-line and sample-mounting systems are illustrated schematically in Fig. XI-5.

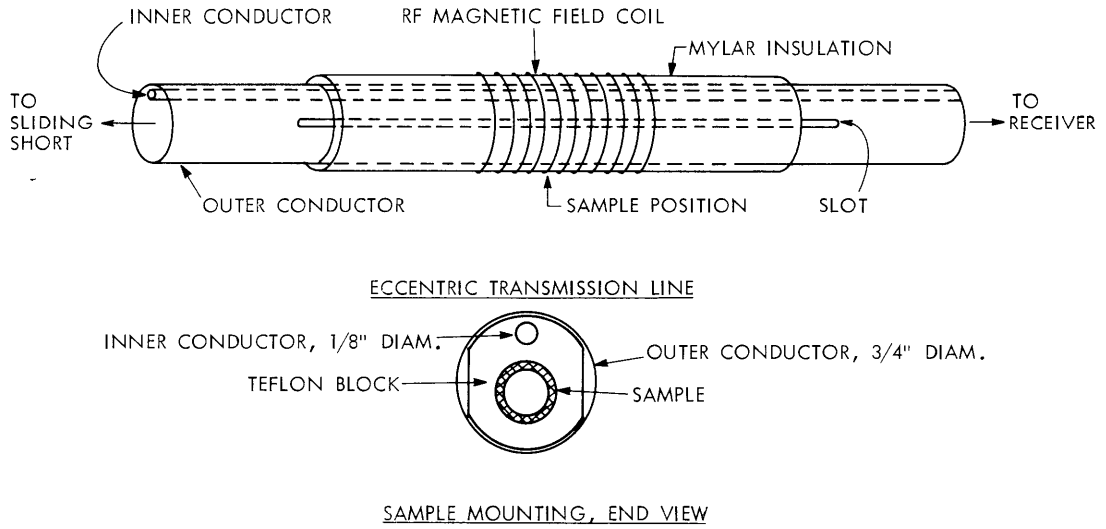

Fig. XI-5. Eccentric transmission line and RF magnetic field coil system, with a detailed view of the sample mounting.

The eccentric transmission line allows observations of microwave emission without the bandwidth limitations of the X-band waveguide previously used. Future observations can easily be made in other microwave frequency bands. Also, because the relatively sharp corners of the waveguide have been eliminated by the use of a circular outer conductor, the problem of dielectric breakdown between the RF magnetic field coil and the transmission line has been reduced. Peak electric fields of ~60 V/cm averaged over the sample can now be obtained before breakdown of the coil structure occurs.

Other changes in the experimental system include the addition of a new electromagnet capable of supplying DC magnetic fields of 10 kG and the modification of the RF pulse generator for improved frequency stability.

Experimental Work

Loop samples were mounted in the eccentric transmission-line system as shown in Fig. XI-5. Liquid nitrogen was used to maintain a sample temperature of 77°K. An electric field was induced in the sample by applying a pulsed 20-MHz RF magnetic field perpendicular to the plane of the loop. A static magnetic field was applied in the plane of the loop. Microwave emission from the sample was observed with a conventional X-band receiver equipped with a synchronous detector.

The peak RF magnetic field was approximately 300 G. Thus it caused a relatively minor perturbation of the DC magnetic field, which was typically in excess of 3000 G whenever microwave emission was observed.

The effects of the orientation of the DC magnetic field, B_o, in the plane of the loop sample deserve some additional comment. For square loops, the field was placed parallel to a diagonal of the square. With this orientation, the magnitude of the components of B_o parallel to and perpendicular to each leg of the square were equal, thereby producing equal magnetoresistance effects in each leg of the square. Except for the regions near the corners of the square, the induced electric field should have been uniform throughout the sample. Near the corners, however, high local electric fields may have existed. Also, the presence of substantial transverse components of B_o near the joints of the soldered square samples could produce large transverse electron velocities as noted by Gueret.[7] The round-loop samples were in principle free from boundaries or inhomogeneities that would have produced large local electric fields or large electron drift velocities. Since indium antimonide exhibits different transverse and longitudinal magnetoresistance effects, and the longitudinal and transverse components of the magnetic field vary continuously around the loop, some spatial variation in the induced electric field strength would be expected. Thus, for both square- and round-loop samples with B_o applied in the plane of the loop, some spatial variation of the induced electric field or electron drift velocity undoubtedly occurred.

Experimental tests of 8 indium antimonide samples were carried out. For those samples that produced microwave emission, output was optimized by adjustment of the position of the sliding short on the transmission line, and plots of the threshold electric field vs DC magnetic field were obtained. "Threshold" was arbitrarily defined at a level approximately 6 dB above the receiver noise level. The "electric field" values given are spatial averages over the sample of values that occurred at the peak of the 20-MHz sinusoidal waveform. The data presented were taken at 9.0 GHz, but similar results were also found at 10.0 GHz.

a. Square Loops with Soldered Joints

Threshold electric and magnetic fields for two square-loop samples containing soldered joints are shown in Fig. XI-6. The values obtained are similar to those found previously,[1,2] but are significantly lower than those required for rod-shaped samples with "good" contacts.[5]

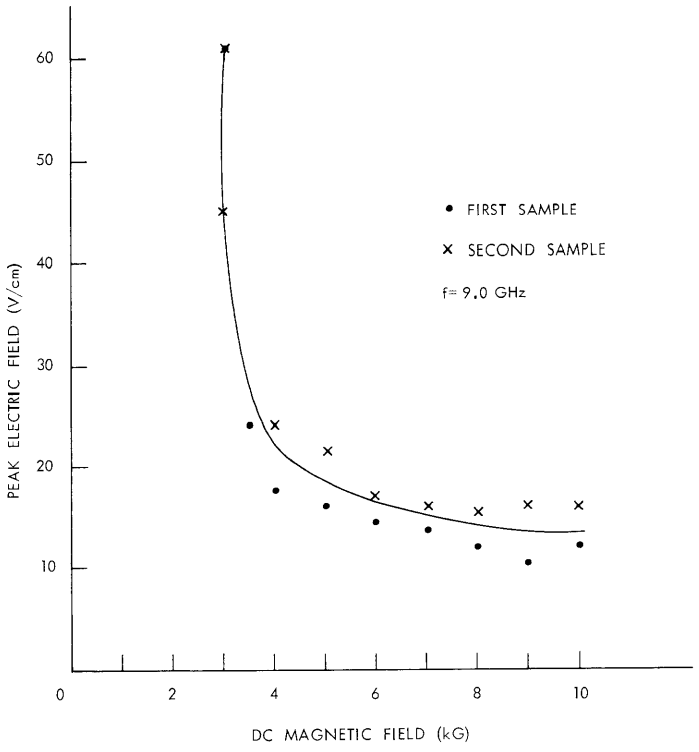

Fig. XI-6. Threshold electric field vs static magnetic field for two square-loop samples with soldered joints. Electric field pulses: 20 MHz sinusoidal burst; 20-μsec duration, 100 pps.

b. Intact Square Loops

Figure XI-7 shows threshold electric and magnetic fields for 2 intact square-loop samples. These samples appeared to be free of cracks or chips both before and after the tests. The corners of the square center hole were quite sharp, however. The threshold electric field for a given magnetic field was in general significantly larger for these samples than for the soldered samples.

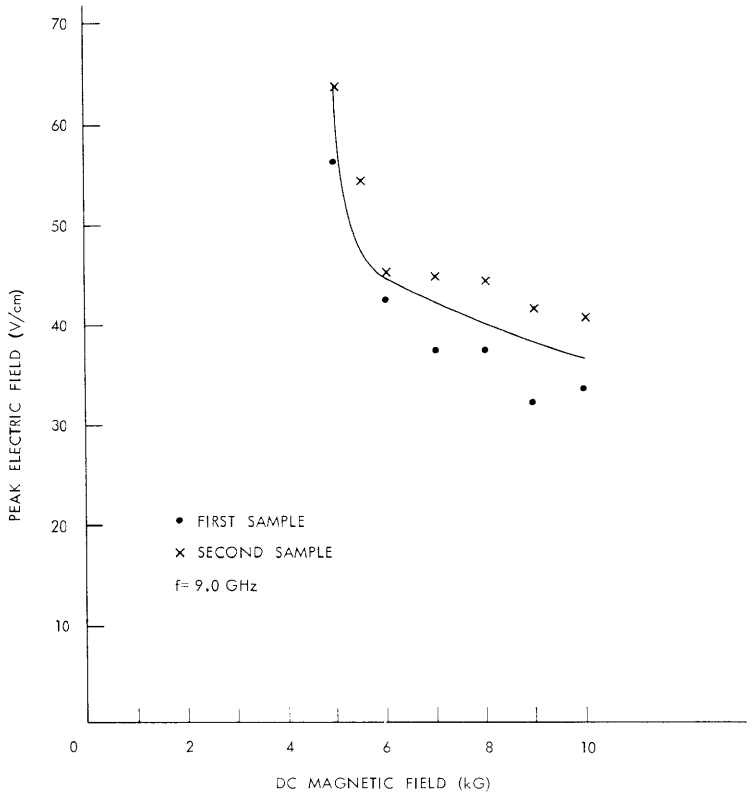

Fig. XI-7. Threshold electric field vs static magnetic field for two intact square-loop samples. Electric field pulses: same as in Fig. XI-6.

c. Round Loops

(i) Loop No. 1 (unoriented)

There was some suggestion of microwave emission from this sample, but the maximum electric and magnetic fields available (60 V/cm and 10 kG) could not produce emission above the threshold level. The surfaces of this sample appeared free of cracks both before and after the tests.

(ii) Loop No. 2 (111) plane

This sample produced copious, but erratic, microwave emission. The emission was a strong function of the polarity and orientation of the static magnetic field. Such threshold data as could be obtained were similar to those found for square-loop samples with soldered joints. After the tests, this sample was found to have a small loose chip of material on its surface, and showed evidence of an additional crack extending into the bulk material.

(iii) Loop No. 3 (111) plane

Electric fields of up to 60 V/cm combined with magnetic fields of up to 10 kG failed to produce microwave emission from this sample. The surfaces of the sample appeared free of cracks or chips both before and after the tests.

(iv) Loop No. 4 (111) plane

This sample did produce emission of approximately the threshold level when subjected to electric and magnetic fields of 60 V/cm and 10 kG, respectively. The emission was somewhat dependent upon the orientation of the DC magnetic field in the plane of the sample. Examination of the sample after the tests showed a crack extending along the outer surface of the sample for a distance of several millimeters.

Conclusions

The data presented here display a fairly definite trend. It becomes more difficult to obtain microwave emission from indium antimonide samples as imperfections are eliminated. At the very least, the "low-field" microwave emission from indium antimonide reported by Buchsbaum, Chynoweth, and Feldmann[3] depends on "bad"[5] contacts or fissures in the material for coupling to the external microwave system. Taking a somewhat stronger position, one might also argue, in view of the present work and that of George,[5] that the "low-field" emission may, in fact, be produced in localized high-field regions that are produced at "bad" contacts, sharp corners, or cracks in the material. Thus "low-field" emission may well be a restricted case of the "high-field" emission reported by Larrabee and Hicinbothem.[8]

Further studies of the emission phenomena reported here are planned. Observations at frequencies outside X-band will be made. Also, round-loop samples will be tested with the static magnetic field applied perpendicular to the plane of the loop, thereby insuring a more uniform spatial distribution of the induced electric field. Attempts will be made to correlate the emission with the condition of the sample surfaces, the crystallographic orientation of the sample, and the distribution of the induced electric field in the sample.

R. N. Wallace

References

1. R. N. Wallace, "Low-Field Microwave Emission from Contactless Indium Antimonide Samples," Quarterly Progress Report No. 87, Research Laboratory of Electronics, M.I.T., October 15, 1967, pp. 121-129.

2. R. N. Wallace, "Effects of Contacts on Low-Field Microwave Emission from Indium Antimonide Loops with Induced Electric Fields," Quarterly Progress Report No. 89, Research Laboratory of Electronics, M.I.T., April 15, 1968, pp. 151-155.

3. S. J. Buchsbaum, A. G. Chynoweth, and W. L. Feldmann, Appl. Phys. Letters 6, 67 (1965).

4. R. N. Wallace, Quarterly Progress Report No. 89, op. cit., see Fig. XII-27, p. 154.

5. E. V. George, "Microwave Instabilities in a Semiconductor Subjected to DC Electric and Magnetic Fields," Quarterly Progress Report No. 91, Research Laboratory of Electronics, M.I.T., October 15, 1968, pp. 154-158.

6. R. N. Wallace, Quarterly Progress Report No. 89, op. cit., see Fig. XII-25, p. 152.

7. P. Gueret, J. Appl. Phys. 39, 2136 (1968).

8. R. D. Larrabee and W. A. Hicinbothem, Jr., Proc. Symposium on Plasma Effects in Solids, Paris, France, 1964.

XI. APPLIED PLASMA RESEARCH*

C. Plasma Physics and Engineering

Academic and Research Staff

Prof. D. J. Rose
Prof. T. H. Dupree
Prof. E. P. Gyftopoulos
Prof. L. M. Lidsky
Prof. W. M. Manheimer
Dr. R. A. Blanken

Graduate Students

N. M. Ceglio, Jr.
H. Ching
D. G. Colombant
M. Hudis
T. R. Hulick
M. A. Lecomte
C. E. Wagner

1. ION ACOUSTIC WAVE PROPAGATION NEAR THE ION-CYCLOTRON FREQUENCY

Recent theoretical investigations[1-3] have predicted strong resonance effects for ion acoustic waves propagating near the ion cyclotron frequency. Two different models for propagation have been treated in these investigations.

1. Plane-wave propagation at an angle to an applied magnetic field in an unbounded plasma.[1,2]

2. Nonplane-wave propagation along a magnetic field in an inhomogeneous plasma column.[3]

We have completed an experimental investigation of ion acoustic wave propagation near and above the ion cyclotron frequency.[4] Waves were excited in a strongly inhomogeneous plasma column. The plasma was produced by a hollow-cathode discharge. Typical plasma conditions had $n_i \approx 10^{13}$ ion/cm^3 and $T_e \gg T_i$. Wave generation was accomplished with a short solenoidal coil placed within the plasma system symmetrically wound around the plasma column. The RF magnetic field of the short coil locally perturbed the applied steady-state B field. The precise mechanism by which the coil launches waves is still not well understood. An axially mobile Langmuir probe was used to detect and measure wave structure.

Wave propagation was investigated in highly ionized Argon and Helium, with most of the work done in Argon. Figure XI-8 shows typical wave structures measured in Argon and Helium. The frequency range that was studied extended from $f \ll f_{ci}$ to $f = 1.6\, f_{ci}$, where f_{ci} is the ion cyclotron frequency. Three different magnetic field conditions were utilized, 680 G, 1150 G, 2300 G. Waves were observed under all of these field conditions. The ion acoustic wave exhibited no dispersion at frequencies near the ion cyclotron frequency (Fig. XI-8b). It was found to propagate along the magnetic field at a constant phase speed

*This work was supported by the National Science Foundation (Grant GK-10472).

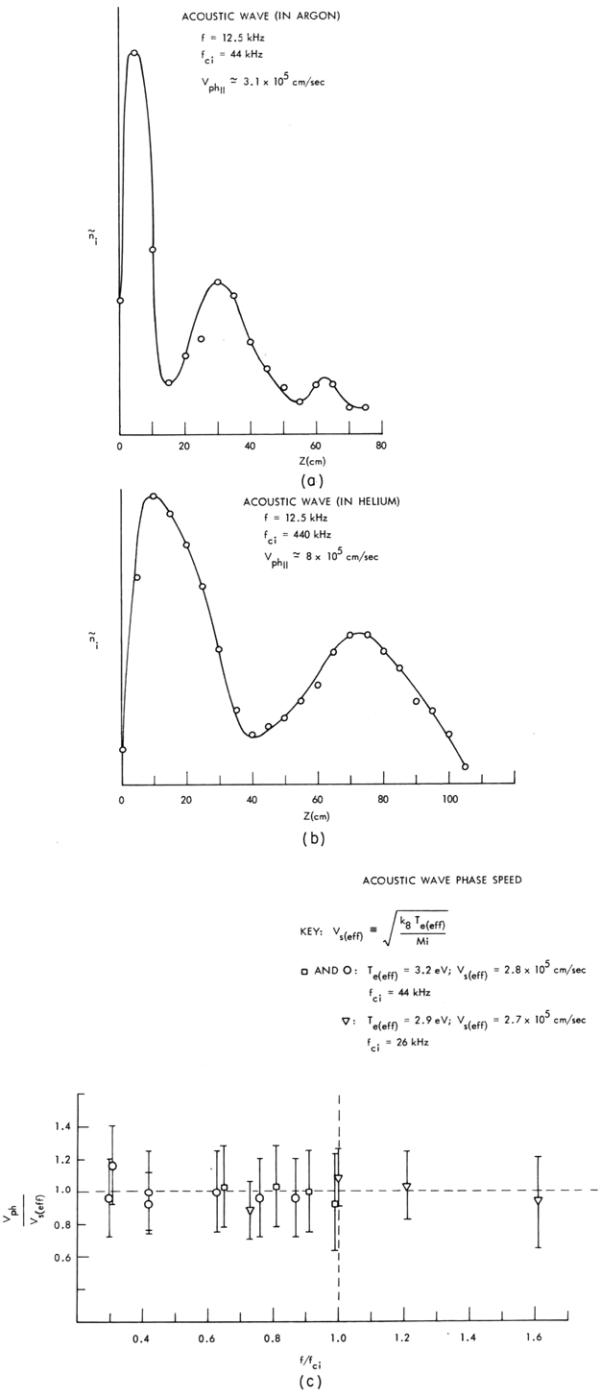

Fig. XI-8. Axial structure for the ion acoustic wave: (a) in Argon; (b) in Helium. $\tilde{n}_i$ is the perturbation in ion density; Z is the distance along the plasma column. (c) The ion acoustic wave exhibited no dispersion over a large frequency range including the ion cyclotron frequency. $V_{ph_{||}}$ is the measured phase speed along the magnetic field; $V_{s(eff)}$ is the effective acoustic speed. Data for three different runs are distinguished by the symbols O, ▽, □.

$$V_{ph_{||}} = \sqrt{\frac{kT_{e(eff)}}{M_i}} \equiv V_{s(eff)}$$

independent of frequency. No cyclotron resonance effects were observed. $T_{e(eff)}$ is the measured electron temperature in the region of strongest radial density gradient.

Spatial attenuation of the ion acoustic wave was measured. Attenuation measurements were hindered by the presence of a fast wave also generated by the coil. The fast wave appears to propagate via an Alfvén-like mechanism with a phase speed of approximately 2×10^6 cm/sec. This is a factor of four below the anticipated Alfvén speed and a factor of ten above the measured ion acoustic speed. The presence of the fast wave interfered with, but did not prohibit, ion acoustic wave measurements. There is qualitative agreement between the measured acoustic-wave attenuation and that expected from ion-ion collision (viscosity) effects.[5] The acoustic-wave attenuation exhibited no resonance effects near the ion cyclotron frequency.

The transverse structure of the ion acoustic wave was also investigated. It exhibited no radial or azimuthal phase dependence. It was standing in both of those coordinates. The precise form of the acoustic-wave radial structure could not be determined because of interference from the fast wave. Nevertheless, the acoustic-wave radial structure appeared to be broad. It peaked off axis.

N. M. Ceglio, Jr., L. M. Lidsky

References

1. G. Joyce and R. Dory, ORNL-TM-2341, June 1968.
2. R. Sugihara and H. Tanaca, ORNL-TM-2345, September 1968.
3. N. Oleson and R. Levin, Phys. Fluids 11, 2251 (1968).
4. N. M. Ceglio, Jr., "Propagation of Ion Acoustic Waves near the Ion Cyclotron Frequency in a Strongly Inhomogeneous Plasma," S. M. Thesis, Department of Nuclear Engineering, M. I. T., May 1969.
5. A. Y. Wong, R. W. Motley, and N. D'Angelo, Phys. Rev. 133, A436 (1964).

2. INSTABILITY OBSERVATIONS IN A BEAM-PLASMA DISCHARGE

We have been using our beam-plasma facility in the mirror configuration to study the physical processes that limit the build-up of a hot-electron plasma in a beam-plasma discharge. In this experiment a pulsed electron beam (10 keV, 1 A, 700 μsec) is shot axially into a 2:1 mirror in the presence of a background gas (helium at pressures of 10^{-5}-10^{-3} Torr). The resultant plasma has been studied both during and after the beam pulse.

Qualitatively, there are two regimes of operation of the beam-plasma discharge. These are shown in Fig. XI-9. At background pressures below 10^{-4} Torr a hot-electron plasma ($T \sim 15$ keV) is produced in addition to a cold plasma ($T \leq 100$ eV). In this regime more than half of the energy of the plasma is in the hot-electron component. Above $p \sim 10^{-4}$ Torr essentially only cold plasma is produced. Here nearly all of the plasma energy is in the cold electrons.

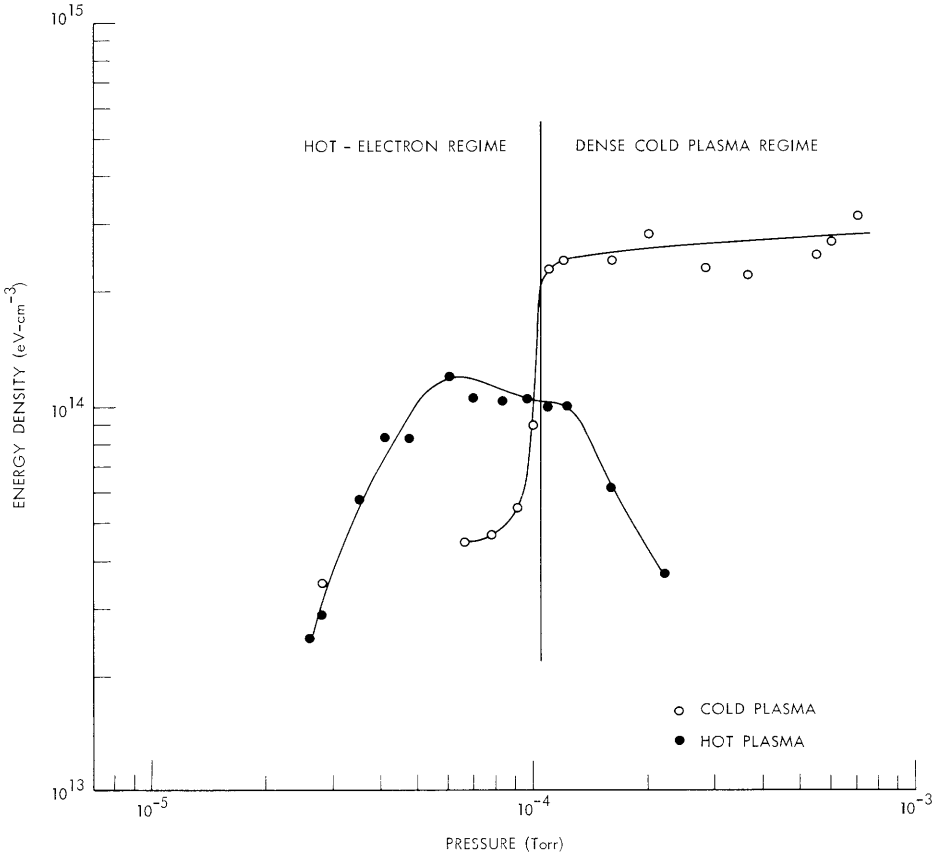

Fig. XI-9. Regimes of operation.

In the hot-electron regime, the hot-electron density increases with background pressure until at $p \sim 8 \times 10^{-5}$ Torr it reaches a maximum value $n_H \sim 10^{10}$ cm^{-3}. As the background pressure is increased the plasma diamagnetism and the x-ray Bremsstrahlung emission become increasingly more turbulent. Typical examples of these signals are shown in Fig. XI-10. Fluctuations in these signals may be as large as a factor of two over a time scale of a few microseconds. After the beam pulse these fluctuations cease, and the plasma decays exponentially with a time constant given by electron-neutral scattering. The fluctuations in the x-ray and diamagnetic signals are

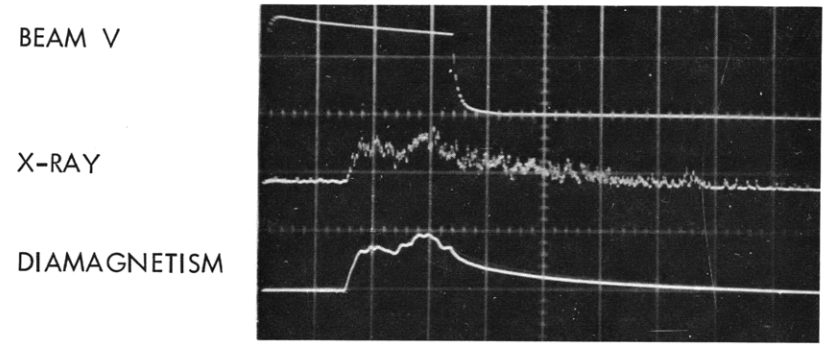

t → 200 μsec/cm

(a)

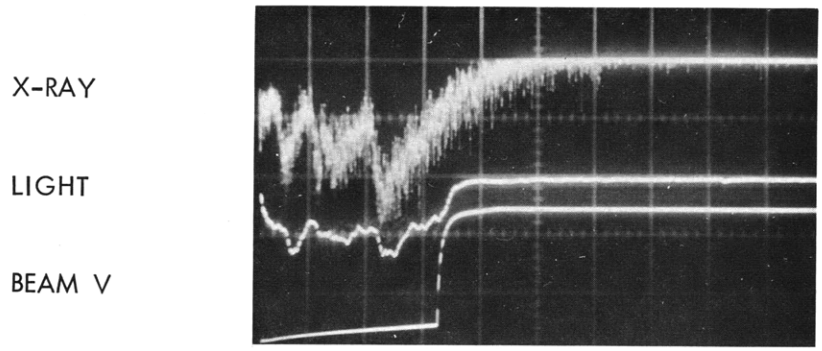

t → 200 μsec/cm

(b)

Fig. XI-10. X-ray, light, and diamagnetic signals.

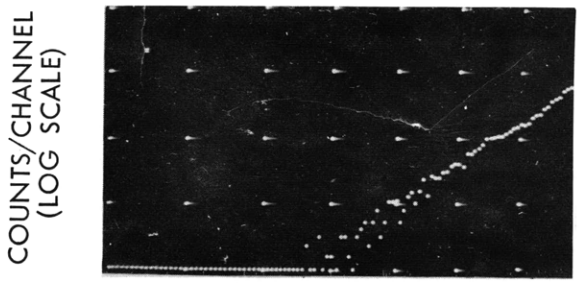

Fig. XI-11. X-ray energy spectrum.

well correlated, but are not well correlated with fluctuations in the visible-light emission from the plasma.

Pulse-height measurements of the x-ray signal indicate that the hot electrons have an exponential energy distribution tail with a characteristic energy of 15 keV, which varies slowly with background pressure and magnetic field intensity. Figure XI-11 shows a typical example of a pulse-height spectrum.

The RF emission from the plasma has been measured around ω_{ce}. Two techniques have been used.

1. The output of an impedance-matched Langmuir probe (Fig. XI-12c) was fed into

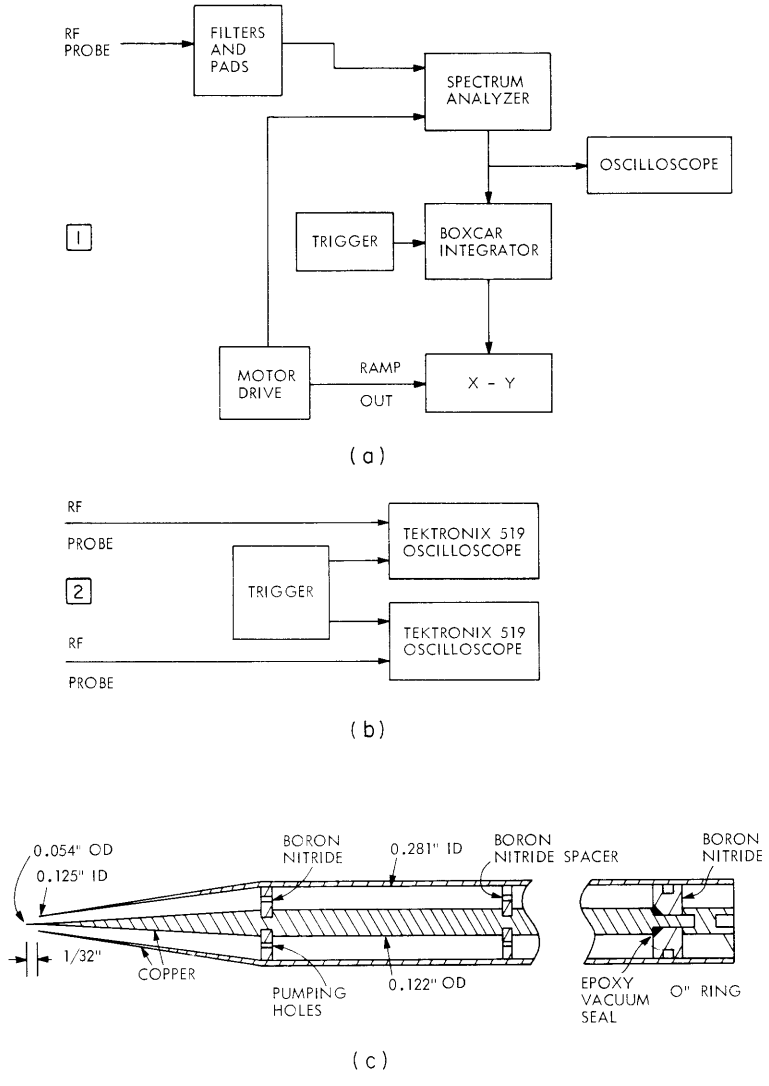

Fig. XI-12. Radiofrequency diagnostics. (a) First technique. (b) Second technique. (c) Impedance-matched Langmuir probe (50 Ω impedance).

a spectrum analyzer which was used as a tunable receiver (Fig. XI-12a).

2. Two impedance-matched probes were fed directly into two Tektronix 519 oscilloscopes. The plasma waves were then observed directly (Fig. XI-12b).

In the vicinity of ω_{ce}, two bands of RF emission were observed during the beam pulse (Fig. XI-13). One band peaks at $\omega \sim 0.6\ \omega_{ce}$ and occurs if and only if there is a large hot-electron density. The RF radiation occurs in spikes (<0.1-μsec duration) which appear in bursts. These bursts are correlated with periods of turbulence in the x-ray and diamagnetic signals and with the peak values of these signals as shown in Fig. XI-14.

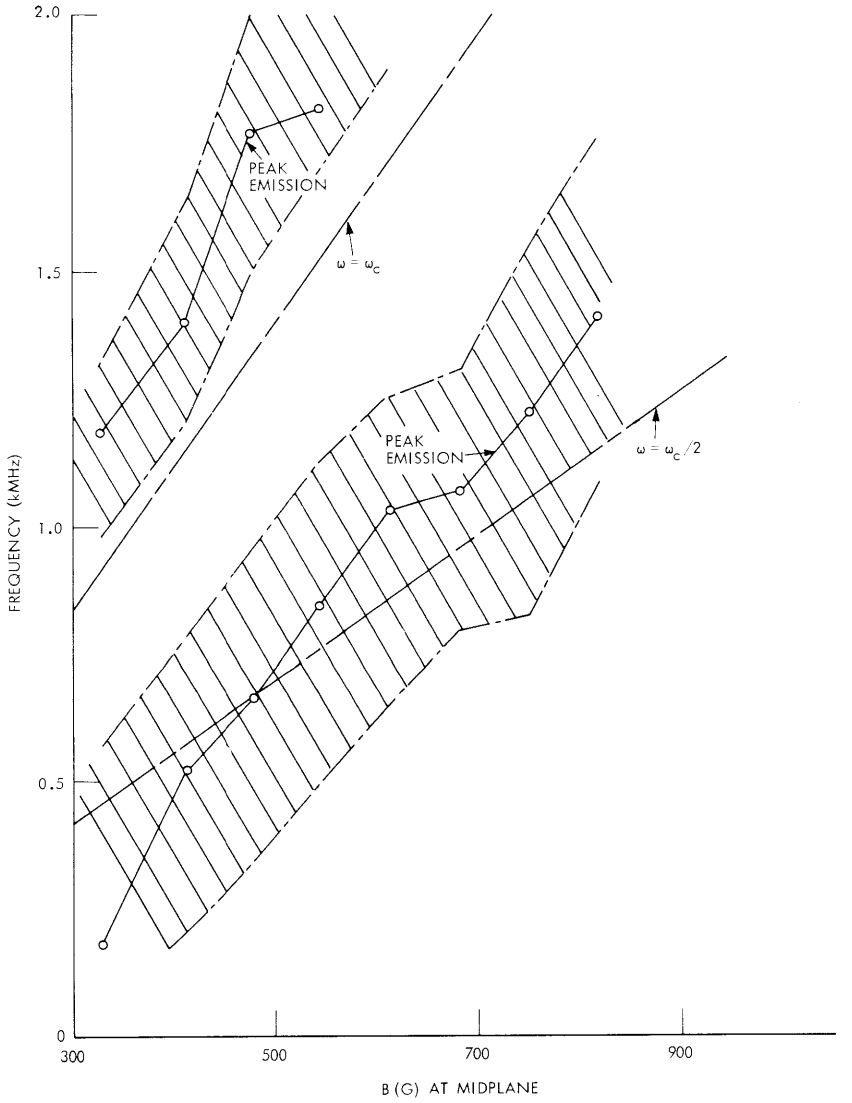

Fig. XI-13. Radiofrequency emission frequency vs B.

The other band occurs at $\omega \sim 1.3\ \omega_{ce}$. This mode seems to be associated with the cold plasma, as it is strongest in the high-pressure regime where there is little hot plasma. The two modes behave quite independently of each other and do not appear to be harmonically related.

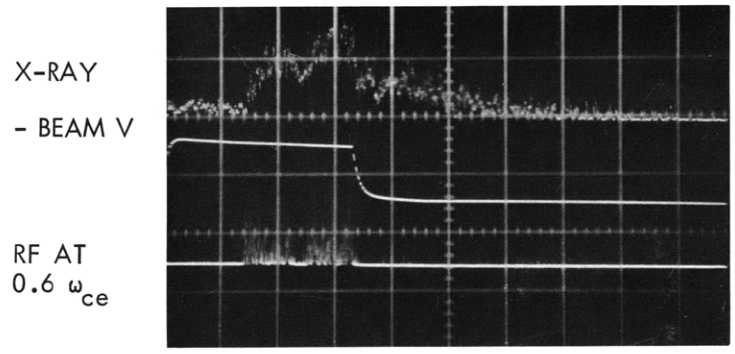

Fig. XI-14. Correlation of the x-ray signal with RF radiation.

Looking at the waves directly with the oscilloscopes, during any one pulse, we see a nearly pure sine wave that is observed to grow or decay and maintain its coherence over many cycles. A few typical waveforms are shown in Fig. XI-15. The frequency

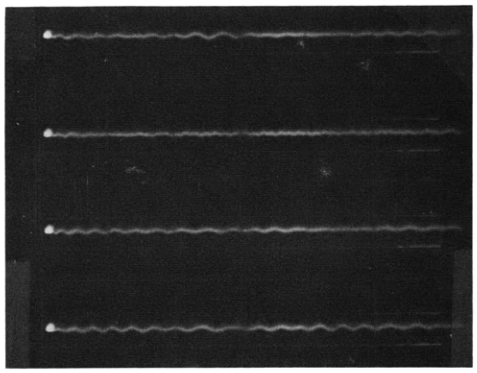

Fig. XI-15. Typical wave trains seen on the oscilloscope.

of the waves observed at a point in the plasma is observed to vary from pulse to pulse. It is important to note, however, that at any one time only one wave (occasionally two) is present at one point in the plasma. The plasma exhibits a high degree of mode

stability. As the wave trains are long, the spikes seen by the spectrum analyzer are likely to be caused by the frequency of the wave sweeping by the narrow-bandwidth receiver frequency. Thus they give the appearance of extremely short spikes in time.

Experiments are in progress to trigger the two Tektronix 519 oscilloscopes simultaneously to observe correlations at different points in the plasma. The waves are observed to be coherent over a few centimeters along a flux tube. We plan to measure $k_\perp$ and $k_\parallel$ of the waves by this technique.

We feel that the 0.6 ω_{ce} mode may be due to a velocity space instability driven by the loss-cone nature of the hot-electron plasma. The dispersion relation for electrostatic waves of this type is[1]

$$D(\omega, \vec{k}) = 1 + \sum_j \frac{\omega_{pj}^2}{\omega_{cj}^2} F_j(\omega, \vec{k}),$$

where the summation j is over particle species, and the term $F_j(\omega, \vec{k})$ is the dispersion term describing the contribution of the j^{th} specie to the wave. We have been investigating a model in which the cold electrons give only a real-negative contribution so that only the hot electrons contribute to the imaginary part of ω, which is necessary for the waves to grow.

C. E. Wagner, L. M. Lidsky

References

1. L. S. Hall, W. Heckrotte, and T. Kammash, Phys. Rev. 139, A1117 (1965).